DETERMINATION OF TIME RELAXATION COEFFICIENT IN LEE MODEL FOR LIQUID HELIUM RELEASE AND DISPERSION

V. Shentsov[1] and D. Makarov[1]
[1]Ulster University, Newtownabbey, BT37 0QB, UK, v.shentsov@ulster.ac.uk, dv.makarov@ulster.ac.uk

ABSTRACT

This study presents the development and comparison of a CFD model to predict dispersion and spills formation of liquid helium (LHe) at cryogenic temperatures. The work is motivated by safety design considerations behind magnetocaloric hydrogen liquefaction system, where LHe is a primary coolant. A contemporary CFD model is essential for assessment of LHe hazards in confined spaces. The CFD setup replicates a controlled experiment involving a 1 L helium spill in a 4.0×3.7×2.7 m enclosure, including humidity variation and sensor-based concentration measurements. The model employs a Volume of Fluid (VOF) approach with the Lee phase-change model and accounts for multiphase species transport. Impact of Lee's model time relaxation parameter on simulation results was studied, the value r=0.1 provided the best agreement with experimental data for lower Dewar vessel elevations during spillage. This value is consistent with the range commonly applied in cryogenic CFD studies, particularly for LH_2 simulations, and aligns with previous findings where in range 0.05–0.2. The model supports safety assessments of LHe releases, evaporation and distribution across a range of incident scenarios with cryogenic applications where LHe is used as a cooling agent.

1.0 INTRODUCTION

Liquid helium is used as a cooling agent in various hydrogen applications including hydrogen liquefaction and storage, which poses safety concerns regarding LHe handling. Accidental releases of inert LHe still may lead to frost bites, asphyxiation and pressure hazards due to rapid vaporisation. Computational Fluid Dynamics (CFD) can be used as tool for simulating these complex multiphase spill, evaporation and dispersion phenomena, thereby enhancing safety assessments, aiding safety design and development of mitigation strategies.

Recent CFD studies have significantly advanced understanding of liquid hydrogen (LH2) behaviour in spill and dispersion scenarios. Middha et al. [1] validated CFD simulations of LH_2 pool spread and evaporation against large-scale experimental data. Holborn et al. [2] quantified hazardous distances from LH_2 pool releases, highlighting the importance of accurately modelling vapor dispersion and atmospheric interaction. Kangwanpongpan et al. [3] applied a Large Eddy Simulation (LES) approach to capture multiphase flash-boiling and pressure recovery phenomena during gaseous releases from pressurised LH2 tank, demonstrating LES superiority over RANS in dynamic events. Giannissi et al. [4] also emphasized the importance of turbulence modelling, applying CFD to assess cryogenic hydrogen dispersion with varying environmental conditions. Recognizing the limitations of fixed evaporation rates, Tan et al. [5] introduced a dynamic correction to the Lee phase change model's coefficient based on local temperature deviation, improving phase-change fidelity. CFD simulations have also extended to cryogenic helium, with Shu et al. [6] providing rare experimental validation data under humid air conditions, relevant for surrogate LH_2 modelling. In parallel, Jazayeri et al. [7] modelled phase change and interface behaviour in cryogenic condensers, using volume of fluid (VOF) method [8] to simulate liquid nitrogen boiling under transient thermal loads. For maritime applications, Choi and Jeong [9] simulated gas dispersion at hydrogen bunkering stations, contributing to safety analysis in emerging hydrogen-fuelled shipping. Giannissi and Venetsanos [10] further compared LH_2 and LNG dispersion behaviour, showing that differences in buoyancy, phase change, and vapor density necessitate dedicated models for each fuel.

In modelling phase transitions, the Lee evaporation–condensation model is widely adopted due to its balance between simplicity and computational efficiency. This model relies on a proportionality

coefficient - time relaxation parameter "r" - that governs the mass transfer rate between phases, which is critical for accurately capturing the evaporation and condensation processes in cryogenic conditions.

The Lee model remains one of the most widely applied approaches for simulating phase change in CFD studies associated with cryogenic species like LH_2. However, the evaporation and condensation coefficients used in these models are highly variable and often tuned based on experimental data or operational conditions. Lv et al. [11] applied the Lee model to investigate thermodynamic behaviour in partially filled LH_2 tanks and emphasized that the evaporation and condensation relaxation parameters (r_{eva}, r_{con}) must be empirically calibrated, though no specific values were reported. In contrast, Zhou et al. [12] tested a set of fixed coefficients 0.05, 0.1, and 0.2 ultimately selecting 0.2 as the optimal value for reproducing experimental pressure rise and liquid level dynamics. Liu et al. [13] used a balanced value 0.1 for both evaporation and condensation in simulations of LH_2 thermal stratification under varying gravity, successfully capturing interface evolution. Zuo et al. [14] extended the model to orbital venting systems, modifying the Lee model with smoothing functions for numerical stability; while they confirmed its use, the specific coefficient range was only described qualitatively. Kangwanpongpan et al. [3] evaluated the effect of Lee model evaporation–condensation coefficients on simulation accuracy. Two coefficient sets were tested: r_{eva}=r_{con}=0.1, and r_{eva}=r_{con}=0.05 While the 0.1 value was initially selected based on common practice in the literature, the simulations revealed an overestimation of minimum pressure during venting. A subsequent run using the lower value of 0.05 s^{-1} resulted in improved agreement with experiments, capturing the pressure recovery effect. Molkov et al. [15] applied a two-phase VOF model with a fixed Lee coefficient of 0.05 to simulate liquid hydrogen refuelling station, capturing transient thermodynamic behaviour. Sivaraman et al. [16] investigated flash boiling during ammonia tank venting, calibrating the Lee model coefficient in the range 0.007–0.1 against experimental pressure and mass release data. Further work of Molkov et al. [17] introduced a multiplier to the Lee model's relaxation time parameter to reflect local vapour volume effects, achieving high-fidelity simulation of ammonia depressurisation.

Broader assessments of boiling and condensation processes have suggested that Lee model coefficients span several orders of magnitude. Review by Kharangate and Mudawar [18] reported the time relaxation parameter values to vary between 10^{-5} and 10^{4} s^{-1}; the authors concluded that the coefficient selection should depend on mesh resolution, interfacial sharpness, and operating conditions. Li et al. [19] modelled gaseous pressurization in LH_2 tanks and used a high evaporation coefficient of 6.0 paired with 0.1 for condensation to capture rapid gas-induced pressurization dynamics. In a no-vent fill scenario, Ma et al. [20] tested a wide coefficient range (0.01 to 100), determining that 0.1 provided the most accurate thermal and mass transfer predictions. Similarly, Kim et al. [21] applied 0.1 as a fixed evaporation coefficient in cryogenic thermosyphon modelling, while dynamically adjusting the condensation coefficient based on density ratios - demonstrating that coefficient flexibility improved model stability and convergence. Finally, Hou et al. [22] simulated LH_2 sloshing in microgravity and used the Lee model in its canonical form to represent interfacial mass transfer; although no explicit coefficient values were given, the authors noted its derivation from the Hertz–Knudsen relation and its role in defining vapor–liquid energy exchange during sloshing and agitation. Together, these studies demonstrate that while 0.05–0.2 remains a widely accepted range for LH_2 evaporation in steady-state CFD, realistic modelling under transient, microgravity, or multiphysics conditions may demand tailored calibration or dynamic treatment of Lee model coefficients. To the best authors' knowledge no similar CFD modelling campaign was performed to obtain time relaxation parameter for LHe and its commonly accepted values still remain to be discovered.

This modelling work is based on the reviewed studies and focuses on CFD model development and simulation results comparison against experimental data on controlled LHe spills. LHe is directly relevant to hydrogen economy development as it is often used alongside LH_2, e.g. in magnetocaloric liquefier systems, where both fluids operate under extreme cryogenic conditions. The safety implications are significant, particularly given helium's low boiling point near 4 K, which will lead to oxygen and nitrogen condensation and solidification, as well as asphyxiation in case of spills in confined environments. A parametric study was therefore conducted to identify suitable Lee model coefficients

for accurately simulating phase change and dispersion of LHe, with the goal of enabling reliable CFD predictions for LHe behaviour in cryogenic systems. This study supports safety analysis of LHe incident scenarios and development of safety strategies for handling cryogenic LHe in hydrogen applications.

2.0 EXPERIMENT SETUP

The experiment by Shu and coworkers on LHe spill [20] was used for CFD simulation results comparison against real world reference data. The LHe spill experiment was performed in an environmental enclosure with dimensions $L \times W \times H$=4.0×3.7×2.7m. Figure 1 presents a photograph and a schematic drawing of the experimental setup in the enclosure. The experimental equipment included:

- LHe spill device made of 1 L Dewar vessel that was "uniformly" emptied during 15 s in a square 200×200 mm pan and depth of 5 mm;
- He and oxygen concentration sensors;
- Data sampler system for data collection and controlled air environment with varying humidity levels (50%, 60%, 70%).

Initial temperature of enclosure walls and air temperature was 20°C. Air supply system in experiment provided wind velocity of 0.2 m/s and varying air humidity levels at left figure shown by green arrows.

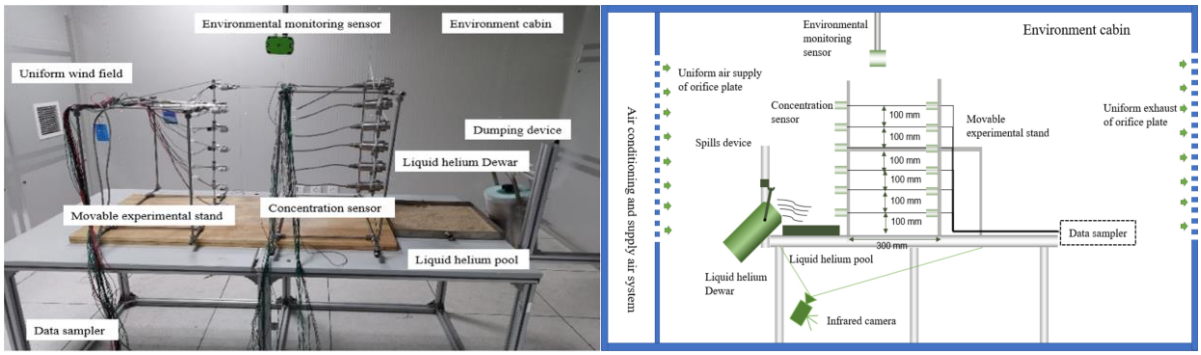

Figure 1. Photograph (left) and schematic drawing (right) of the experimental setup [23]

3.0 CFD MODEL DESCRIPTION

3.1 Governing equations and numerical details

Governing equations included transient mass, momentum, energy and species conservation equations. VOF method was used to track phases and phase interface. Gaseous helium (GHe) and LHe densities and specific heat capacities were adopted from NIST real gas tables [24]. Realisable k-ε model with standard wall functions was used to simulate effect of turbulence. The species included H_2O, N_2 and O_2 in gaseous, liquid and solid forms and He in gaseous and liquid forms with phase transitions. The initial and boundary conditions such as pressure, temperature, humidity, and velocity were specified as per experimental setup [23]. ANSYS Fluent 2020 R2 was used as a CFD engine with pressure-based implicit solver, SIMPLE method for pressure-velocity coupling, pressure discretisation method PRESTO, 2nd order Central Difference scheme for discretisation of diffusion terms, 2nd Order Upwind numerical scheme for discretisation of convective terms in momentum conservation equations, 1st order upwind scheme - for convective terms in equations for turbulent kinetic energy and its dissipation rate, energy and all species. Compressive scheme was set for volume fraction.

Helium liquefaction temperature 4.22 K is below of both O_2 and N_2 liquefaction temperatures 90.2 K and 77.4 K respectively, and lower than O_2 and N_2 solidification temperatures 54.4 K and 63.1 K respectively. Thus air contact with LHe may result in condensation and then solidification of all major species present in air – N_2, O_2 and H_2O. To provide solidification impact on energy balance the CFD model accounted solidification in the same manner as liquefaction – Lee model was used for mass transfer mechanism, while thermal properties of solid O_2 and N_2 were assigned to liquid phases created

on purpose in CFD model. Such treatment accounts solidification impact on energy balance, but simplifies fluid dynamics treatment of solid phases (i.e. in fact the "solid" phases are similar to liquid phases). Downside of this simplification is inability of the presented CFD model to predict accumulation of solid phases as they are the same subject for convective transport as liquids and easily washed away from solidification location.

3.2 GHe specific heat capacity

GHe specific heat capacity $C_{p,G}$ was approximated using polynomial functions based on NIST database [24]**.** To provide better accuracy two approximation equations were created for different temperature ranges: Eq. (1) is applicable in the temperature range 4.2238 - 20.15K, and Eq. (2) is applicable in the range 20.15 - 300.15K,

$$C_{p,G} = 0.0242x^6 - 1.917x^5 + 61.37x^4 - 1{,}015.5x^3 + 9{,}142.1x^2 - 42{,}457x + 85{,}103\,, \quad (1)$$

$$C_{p,G} = 4 \cdot 10^{-12}x^6 - 4 \cdot 10^{-9}x^5 + 4 \cdot 10^{-6}x^4 - 0.0004x^3 + 0.0462x^2 - 2.908x + 5{,}269.7. \quad (2)$$

Specific heat capacity of LHe was specified as a constant value $C_{p,L}$=4,809.2 J/kg·K, for the temperature range 4.15–4.2238 K. This simplified treatment was deemed appropriate given the narrow temperature window relevant to the simulated evaporation process.

3.3 Calculation domain and numerical mesh

Figure 2 shows calculation domain and numerical grid at side boundary (left) and in the vertical cross-section (right). Calculation domain was discretised using 170,519 polyhedral control volumes (CVs) and adequately captures the experimental setup geometry. The area around sensors and release point as well as the pan surface were further refined to allow better performance and capture temperature gradients near the spill and accurate resolution of concentration while saving simulation time. The dewar vessel was also added to the geometry to allow as close as possible representation of the experimental geometry to provide accurate simulation of flow and turbulence formation in front of the sensors. Inflow and outflow surfaces were given as in experimental description [23] and was a square of 1.8x1.8 m on opposite side of the walls.

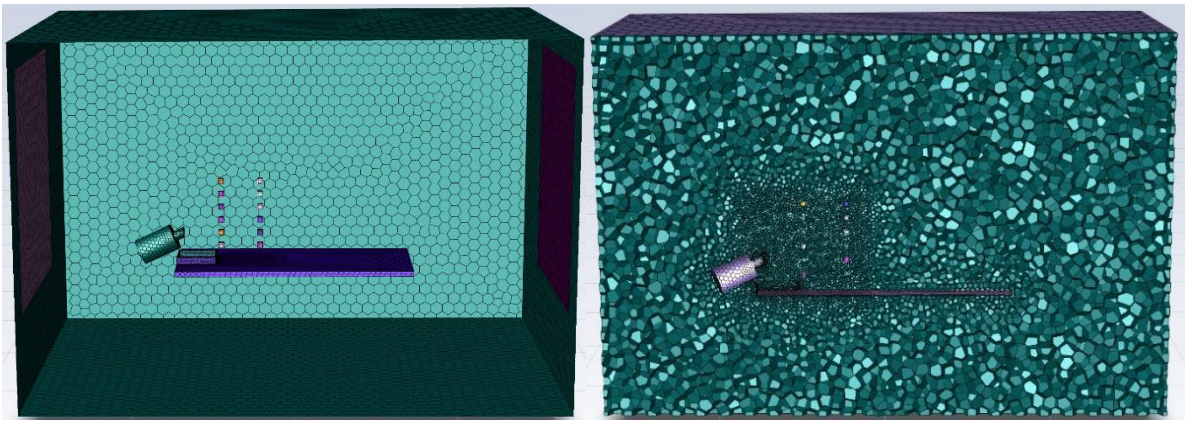

Figure 2. Calculation domain and numerical grid: boundary mesh (left), vertical cross section (right)

3.4 Initial and boundary conditions

The velocity inside the domain was initialised at 0.2 m/s via steady state simulation before the spill started in a transient mode. This was done to allow stabilisation of the flow across the room and to make sure that this won't affect the dispersion dynamics of the release stage. The air composition and relative humidity level of 50% resulted in the following species volume fractions: $X(O_2)$=0.22834, $X(N_2)$=0.76445, $X(H_2O)$=0.00721. The initial temperature of the inflow air was set as per experiment

and was equal to 293.15 K. The LHe spill was realized via circular boundary of 80 mm in diameter, which was approximated from the experimental setup in Figure 1. Constant inflow rate uniformly distributing 1 L of LHe over the period of 15 seconds resulted in mass flow rate of 8.3 g/s.

4.0 RESULTS AND DISCUSSION

4.1 Parametric study for Lee's model time relaxation parameters

Parametric study to identify the best Lee's time relaxation parameter value for model performance was undertaken first. To the authors' knowledge, no published data reporting Lee coefficients for LHe are available. Therefore, the following values commonly used in LH_2-related studies were taken as a reference for the parametric study: 0.005, 0.05, 0.01, 0.1.

Figure 3 shows comparison of experimentally measured GHe volume concentration (shown by black solid lines across various heights) with simulation results (colour coded solid lines) obtained with different time relaxation parameter values (0.005 – purple, 0.05 – green, 0.01 – red, 0.1 – blue). Though the qualitative CFD solution behaviour is similar to the experimental trend across all tested values of time relaxation coefficient, the best quantitative agreement is provided for the time relaxation coefficient r=0.1. With this value the CFD model replicates key dispersion characteristics of cryogenic helium release across all sensors' heights. It is particularly remarkable that the model reproduced GHe concentrations close to experimental measurements at lower sensor heights (100–300 mm), which suggests that r=0.1 value allows correct capturing phase change dynamics in the LHe pan. Therefore, all further analysis will be performed for simulations with Lee time relaxation parameter value r=0.1.

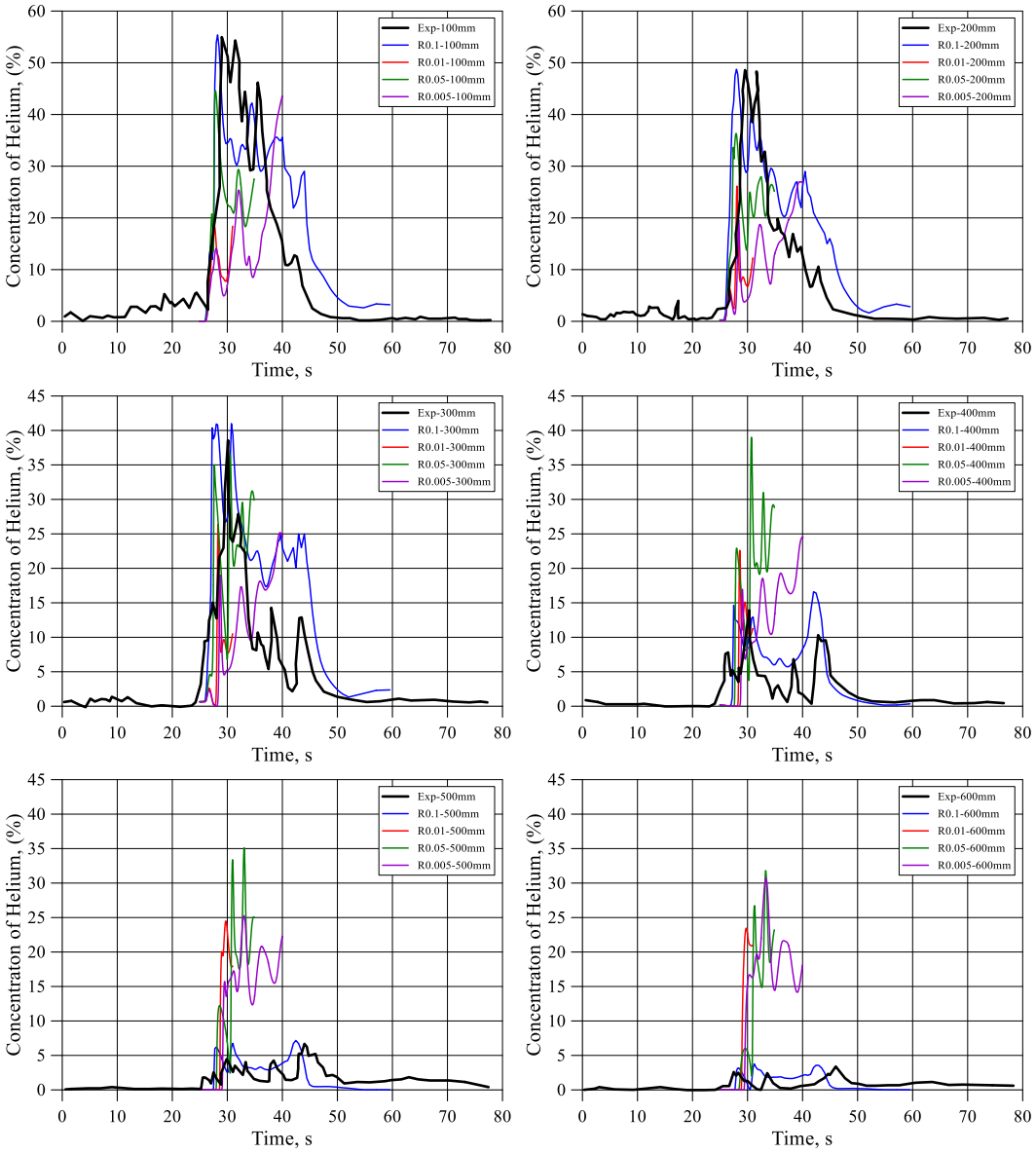

Figure 3. Comparison of experimental (black) and simulated (colour) helium concentration (vol.) with time relaxation parameter values 0.1, 0.05, 0.01, 0.005, sensor heights 100-600 mm.

4.2 Concentration dynamics

To further analyse the dispersion behaviour, Figure 4 presents a series of helium vol. concentration snapshots in vertical cross-section demonstrating GHe plume development at times *t*=1, 5, 10, 15, 20, 24, 30 and 36 s. These images capture the spatial development of the cryogenic GHe cloud from the moment of LHe release through the full evaporation cycle and into the post-spill dispersion phase. At *t*=1 s the release has just begun, and helium remains concentrated near the Dewar vessel outlet. By *t*=5 s the buoyancy-driven flow well-pronounced and should start distorting the lateral flow pattern established in the experimental enclosure before the spill start. At *t*=15 s the helium plume reaches its maximum horizontal and vertical size, which is likely due to a combination of continued evaporation, mixing with ambient air, and reduced density over time. At t=15 s the spillage ends, and the cloud gradually dilutes and disperses. At *t*=20 s GHe cloud is already barely visible (mostly under the table) and by *t*=36 s it practically disappears with residual gas moving upward and outward. The visualised concentration fields confirm that the model captures both transient accumulation and subsequent dissipation effectively. The consistency between simulated and observed plume development further validates the selection of 0.1 as the appropriate Lee coefficient under these conditions.

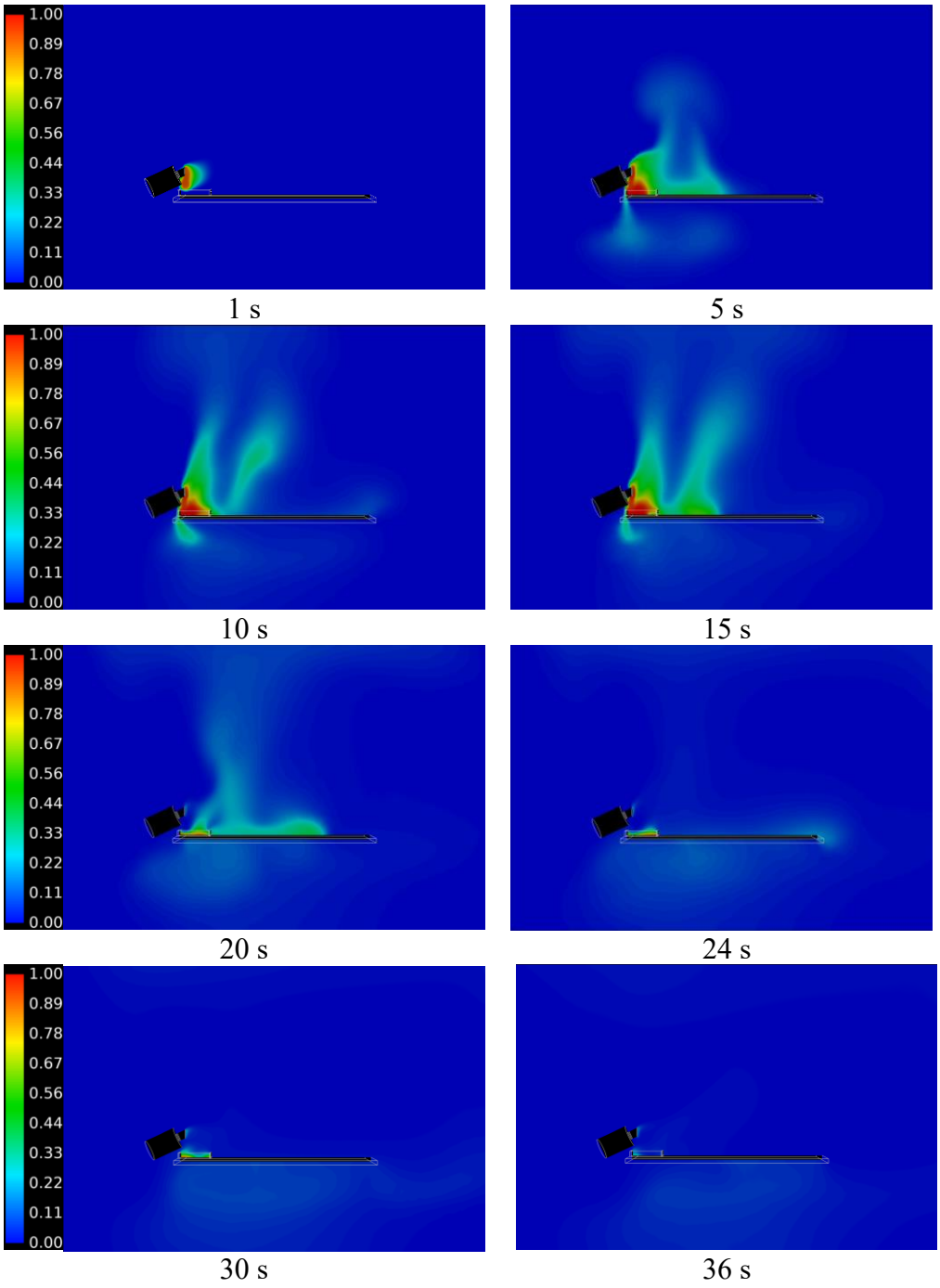

Figure 4. Dynamics of GHe vol. concentration distribution in vertical domain cross-section

4.3 Temperature dynamics

Figure 5 shows temperature distribution evolution. At initial moment, *t*=1 s, LHe doesn't reach the tray. As LHe volume fraction in the spill pan increases so does the cooler but lighter He plume above the pan. During the period between *t*=5 and 15 s the LHe spill evaporates and forms a cold stratified zone near the spill pan, which then expands further spreading along the table and beneath. At *t*=15 s the cooler GHe plume is substantially larger than at *t*=5 s and at *t*=10 s, which is in line with GHe distribution in Figure 4. While helium gas at cryogenic temperatures is initially denser than air and tends to sink or remain near the spill zone, its continued evaporation and mixing with ambient air gradually reduces its density, allowing buoyancy effects to become more pronounced over time. LHe spillage ends at *t*=15 s

and after that time LHe fraction decreases together with GHe plume. At t=24 s and beyond the GHe plume and associated with it cooler temperature area both are practically non-existent.

The temperature field behaviour appears to be physically correct and feasible including transient temperature gradients, which were especially sensitive to humidity level, as were described in experiment [23]. However, in absence of the transient experimental measurements of temperature for all humidity levels it is difficult to provide quantitative assessment of simulated temperature distribution, though we can rely on the correct helium concentration dynamics, which typically implies the correct temperature dynamics as well.

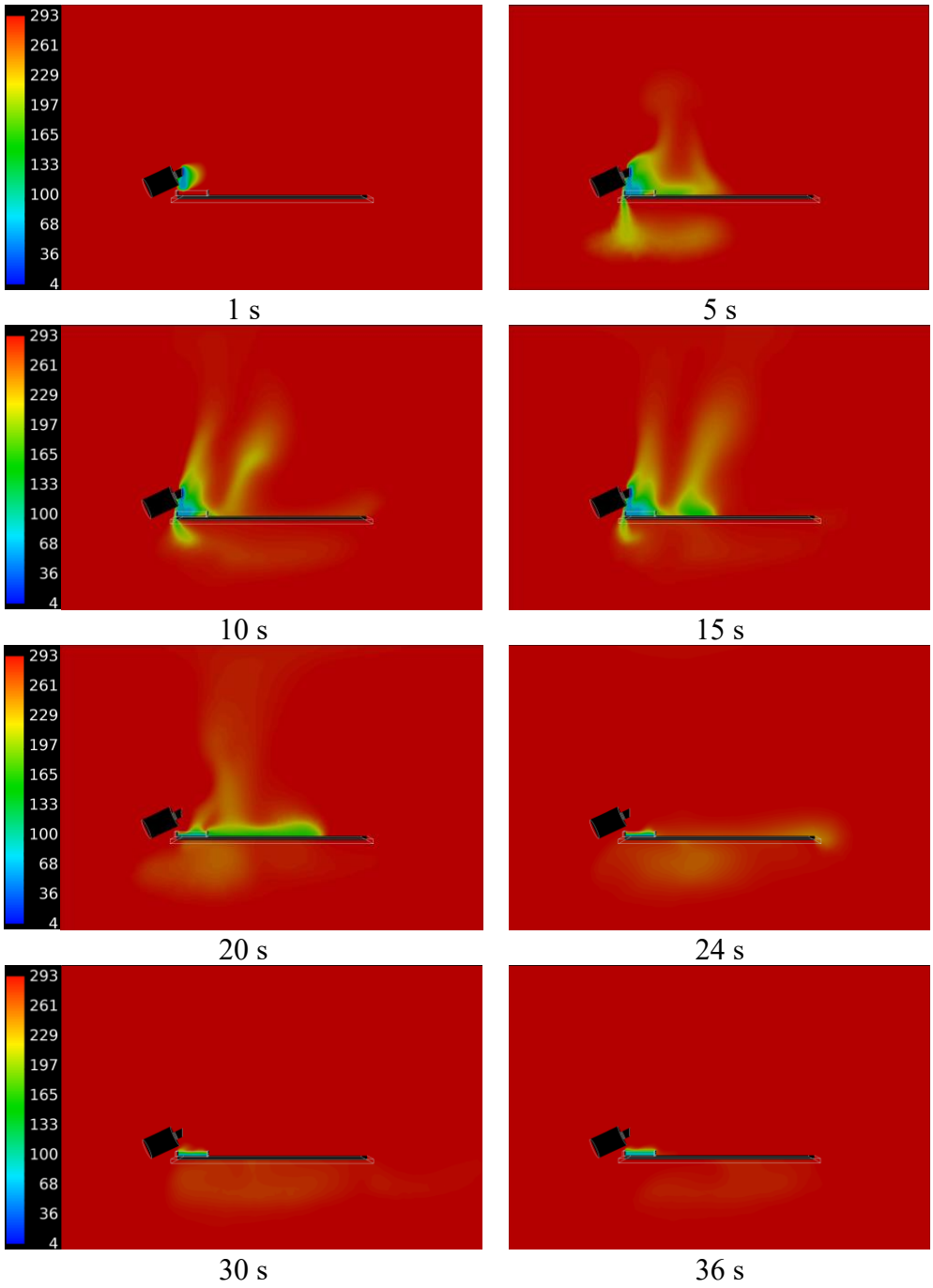

Figure 5. Dynamics of temperature distribution in vertical domain cross-section

4.4 Velocity field dynamic

Velocity field analysis showed consistent plume rise and lateral dispersion trends in the entire LHe spill duration. Figure 6 shows velocity vector distribution in the domain vertical cross section at different times. At time t=1 s it can be seen that the flow is quasi steady-state following the initial condition and within 0.2 m/s as per experimental description. At later times the spilled LHe undergoes phase transition generating large GHe quantity, which distorts the flow field. Both buoyancy-driven upward motion and then GHe lateral spread break the uniform transfer flow pattern existing at initial moment. Based on CFD results - at t=24 s there is no helium plume from evaporation, hence we may suggest that LHe evaporation is complete, and at t=36 s, it is possible to see that the flow starts to establish the pattern similar to that which existed at the initial moment.

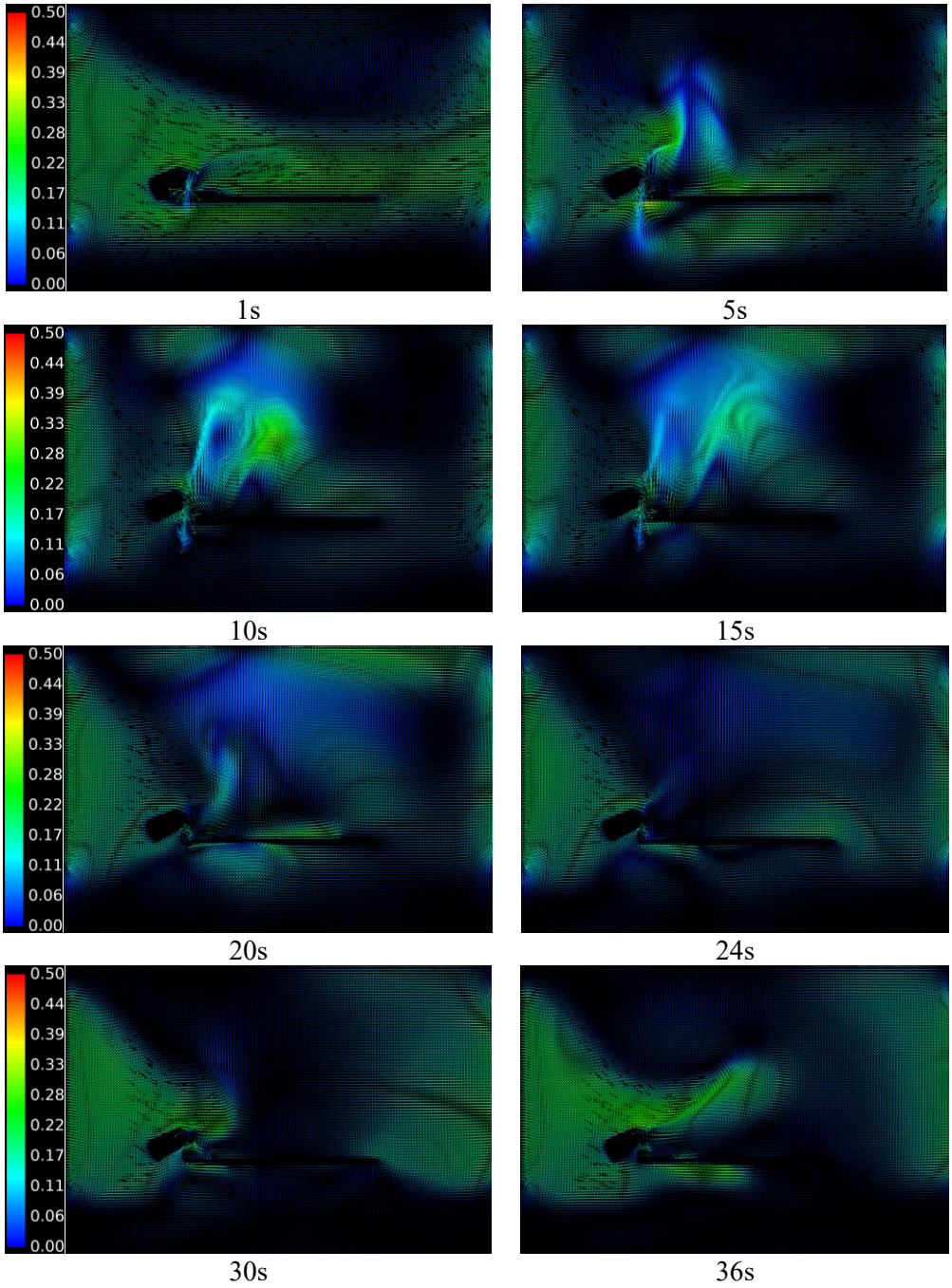

Figure 6. Dynamics of velocity vector field in vertical domain cross-section.

4.5 Formation of liquid and solid oxygen and nitrogen

The developed CFD model allows for oxygen, nitrogen and water condensation and freezing near the spill surface due to extreme cooling from LHe presence and evaporation at temperatures close to 4.15 K. The presence of solid oxygen (SO_2) introduces safety concerns, including flow obstruction in pipes and increased flammability risk if SO_2/LO_2 (liquid oxygen) re-vaporisation leads to oxygen-enriched atmosphere. To the best of authors knowledge there are no published CFD studies addressing analysis of O_2 and N_2 liquefaction and solidification as a results of incident with cryogenic liquids.

The extremely low LHe temperature of 4.15 K creates favourable conditions for ambient air O_2 and N_2 condensation and solidification. Figure 7 illustrates the time-resolved distribution of liquid oxygen (LO_2) vol. fraction near the spill region during the initial 24 seconds of the process. As shown, O_2 rapidly condenses within the first seconds, forming a thin liquid film along the surface adjacent to the spill pan bottom. The condensation process intensifies as LHe-induced cooling reaches a broader area of the pan. By t=15 s a stable layer of condensed LO_2 is observed at the pan bottom increasing up to 24 s, concentrated beneath the spill area. This localized LO_2 accumulation may pose safety hazards due to potential oxygen-enrichment zones where ignition sensitivity could increase. The simulation confirms the developed CFD model capability to predict O_2 condensation dynamics with spatial and temporal resolution relevant to incident scenarios in cryogenic applications.

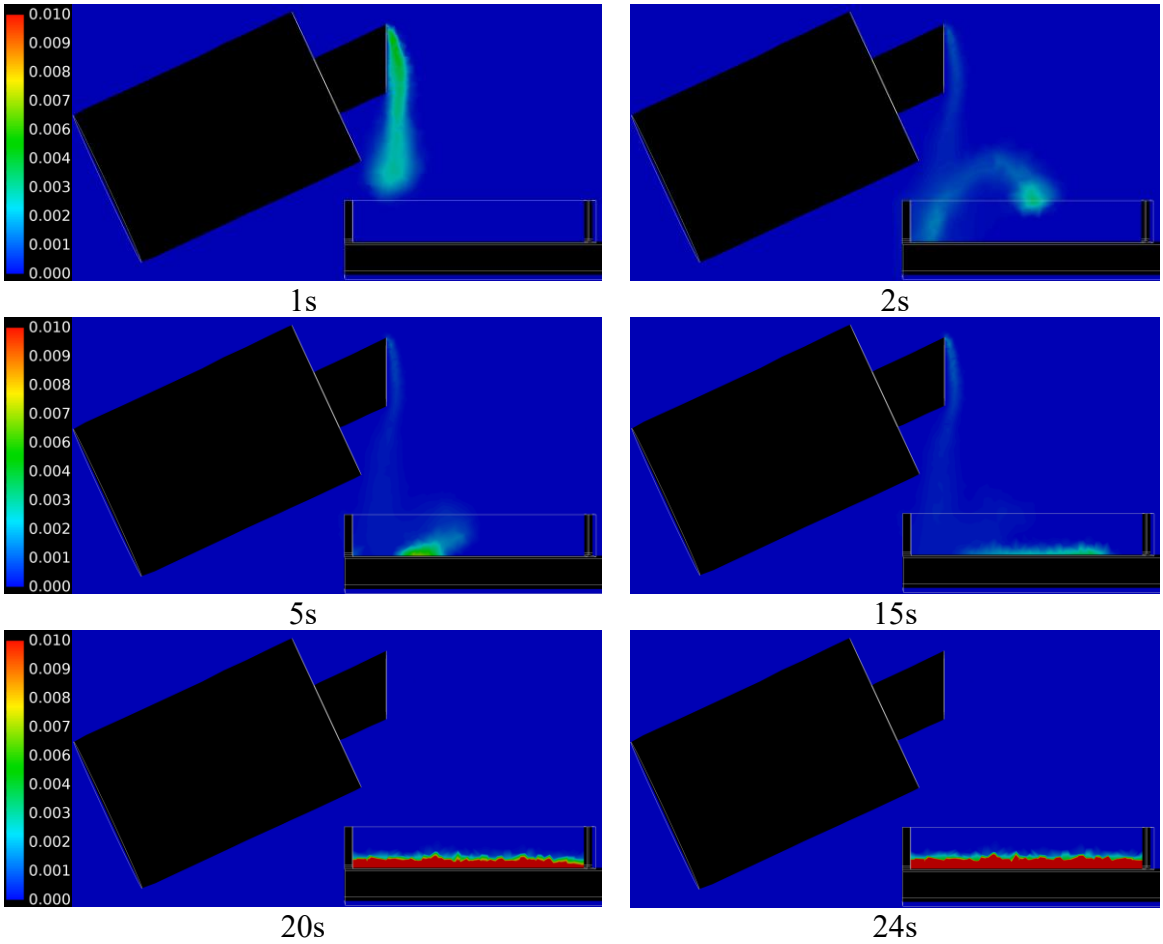

Figure 7. Dynamics of liquid oxygen formation, vol. fraction.

In addition to liquid phase condensation, the model also predicts the formation of solid oxygen (SO_2) and solid nitrogen (SN_2). Figure 8 presents comparison dynamic of SO_2 (left) and SN_2 (right) vol. fraction distribution in the vertical domain cross-section. The figure shows onset and development of phase transition within the first 16 s following the spill. Initial traces appear

as soon as LHe enters the domain and ca be seen from 1 s, concentrated near the release surface where temperatures approach the O_2 freezing point (54.4 K) and N2 (63.15 K). The deposition continues to be observed through t=1 to 15 s, with the densest accumulation around the Dewar outlet and the pan boundary. By t=16 s SO_2 concentration practically diminishes, indicating that a persistent cryogenic zone capable of maintaining O_2 sub-freezing temperatures for extended durations is present only during the release period while traces of SN_2 still remain at the pan bottom. These simulation results underscore the importance of accounting for cryo-condensation and solidification in safety assessments, especially in confined or poorly ventilated systems, where the accumulation of solidified oxygen or nitrogen may pose hazards such as restricted flow paths, structural stresses from phase volume changes, or the formation of oxygen-enriched environments that significantly increase fire or explosion risks.

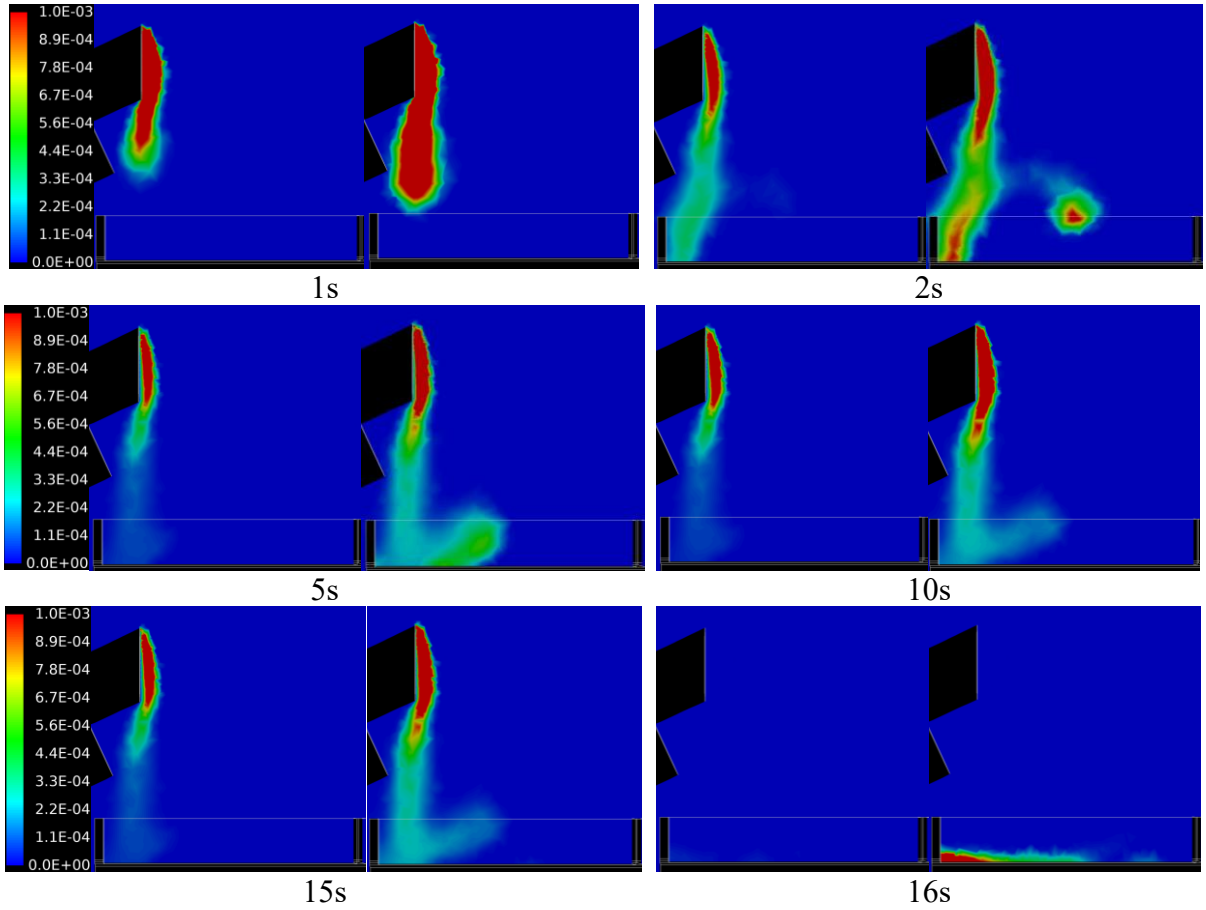

Figure 8. Comparison dynamics of solid oxygen(left) and solid nitrogen(right) formation, vol. fraction.

4.0 CONCLUSIONS

The *originality* of the paper is in development of a multiphase CFD model for liquified helium spill, evaporation and dispersion accounting liquefaction and solidification of oxygen, nitrogen and water vapour (not presented) contained in air. The model correctly represents liquid to solid phase transition, but rests on simplification of solid phases treatment in momentum equation as actually liquid phases, which allows for their convective transport. Parametric simulation campaign, aimed at finding the optimal Lee model time relaxation parameter for helium evaporation, was performed for the first time too. Time relaxation coefficient value r=0.1 was found to provide the closest to the experiment helium vol. concentration dynamics across the entire range of experimental sensors' heights.

The *rigour* of the study is in (1) comparison of simulated and experimentally measured dynamics of helium vol. concentration distribution, and (2) interpretation of the simulation results for helium, temperature, velocity fields, and spatial-temporal distribution of solid oxygen and nitrogen, used to illustrate consistency with expected behaviour from a conceptual physical model, though without direct experimental comparison. The obtained simulation results are close to experimental observations, physically viable and consistent, which confirms robustness of the chosen modelling approach.

Significance of the study is in the availability of the developed model for analysis of hazards and associated risks in hydrogen applications using helium as a cooling agent. The model is capable to reproduce behaviour of liquified and gaseous cryogenic helium. This includes liquid and solid oxygen and nitrogen formation resulting from spill, evaporation and dispersion of liquid helium, which has extremely low saturation temperature 4.15 K. Such cryo-condensation and solidification phenomena are rarely quantified in CFD studies, yet they are critical for realistic safety assessments of LH_2 and LHe scenarios. The presence of condensed or solidified oxygen can locally enrich the atmosphere in oxidisers, increasing the risk of ignition or violent combustion if flammable gases are later introduced. Additionally, accumulation of solids may obstruct ventilation paths or instrumentation. The modelling approach used here, based on the Lee model with thermophysical properties adapted for O_2 and N_2 solidification, is directly extendable to LH_2 spills, which can also induce air condensation and freezing under certain conditions, especially in confined spaces.

While the absolute inventory is limited, the physical processes captured: rapid phase change, buoyancy-driven dispersion, and condensation are fundamentally the same in larger-scale LH_2 incidents. The modelling approach, including phase change treatment and thermophysical property handling, is scalable and directly applicable to LH_2. Future simulations will incorporate realistic LH_2 inventories, infrastructure geometries, and varying ventilation to assess hazard zones and develop engineering safety strategies. The next stage of this work involves applying the validated CFD model to analyse incident scenarios within the magnetocaloric hydrogen liquefaction (MCHL) system. This includes assessment of cryogenic spills, dispersion, and oxygen condensation/solidification in confined geometries, supporting hazard identification and development of safety strategies specific to the MCHL environment.

5.0 ACKNOWLEDGEMENTS

This research has received funding from the Clean Hydrogen Partnership under grant agreement No. 101101461 (HyLICAL). The project is supported by the Clean Hydrogen Partnership and its members. UK participant in Horizon Europe Project HyLICAL is supported by UKRI grant No. 10066462 (University of Ulster). The authors are grateful to the Engineering and Physical Sciences Research Council (EPSRC) of the UK for support through the Tier 2 High-Performance Computing resources provided by the Northern Ireland High-Performance Computing (NI-HPC) facility.

6.0 REFERENCES

1. Middha, P., Ichard, M., and Arntzen, B.J. Validation of CFD modelling of LH2 spread and evaporation against large-scale spill experiments. *International Journal of Hydrogen Energy*. 36, no. 3. 2620–2627. 2011
2. Holborn, P.G., Benson, C.M., and Ingram, J.M. Modelling hazardous distances for large-scale liquid hydrogen pool releases. *International Journal of Hydrogen Energy*. 45, no. 43. 23851–23871. 2020
3. Kangwanpongpan, T., Makarov, D., Cirrone, D., and Molkov, V. LES model of flash-boiling and pressure recovery phenomena during release from large-scale pressurised liquid hydrogen storage tank. *International Journal of Hydrogen Energy*. 50. 390–405. 2024

4. Giannissi, S.G., Venetsanos, A.G., Markatos, N., and Bartzis, J.G. CFD modeling of hydrogen dispersion under cryogenic release conditions. *International Journal of Hydrogen Energy*. 39, no. 28. 15851–15863. 2014
5. Tan, Z., Cao, Z., Chu, W., and Wang, Q. Improvement on evaporation-condensation prediction of Lee model via a temperature deviation based dynamic correction on evaporation coefficient. *Case Studies in Thermal Engineering*. 48. 103147. 2023
6. Shu, Z., Lei, G., Liang, W., Dai, W., Lu, F., Zheng, X., and Qian, H. Experimental investigation of hydrogen dispersion characteristics with liquid helium spills in moist air. *Process Safety and Environmental Protection*. 162. 923–931. 2022
7. Jazayeri, S., Pourahmad, A., Abdollahi, S.A., Hassanvand, Amin., Alobaid, F., and Aghel, B. Experimental Investigation and CFD Simulation of Cryogenic Condenser. *Processes*. 11, no. 6. 1845. 2023
8. Hirt, C.W. and Nichols, B.D. Volume of fluid (VOF) method for the dynamics of free boundaries. *Journal of Computational Physics*. 39, no. 1. 201–225. 1981
9. Choi, S. and Jeong, B. CFD simulation of gas dispersion at hydrogen bunkering station. *Journal of International Maritime Safety, Environmental Affairs, and Shipping*. 7, no. 4. 2261350. 2023
10. Giannissi, S.G. and Venetsanos, A.G. A comparative CFD assessment study of cryogenic hydrogen and LNG dispersion. *International Journal of Hydrogen Energy*. 44, no. 17. 9018–9030. 2019
11. Lv, R., Huang, Y., and Wu, J. Thermodynamic analysis of partially filled hydrogen tanks in a wide scale range. *Applied Thermal Engineering*. 193. 117007. 2021
12. Zhou, R., Zhu, W., Hu, Z., Wang, S., Xie, H., and Zhang, X. Simulations on effects of rated ullage pressure on the evaporation rate of liquid hydrogen tank. *International Journal of Heat and Mass Transfer*. 134. 842–851. 2019
13. Liu, Z., Li, Y., and Zhou, G. Study on thermal stratification in liquid hydrogen tank under different gravity levels. *International Journal of Hydrogen Energy*. 43, no. 19. 9369–9378. 2018
14. Zuo, Z., Jiang, W., Qin, X., and Huang, Y. Numerical investigation on full thermodynamic venting process of liquid hydrogen in an on-orbit storage tank. *International Journal of Hydrogen Energy*. 45, no. 51. 27792–27805. 2020
15. Molkov, V., Ebne-Abbasi, H., and Makarov, D. Liquid hydrogen refuelling at HRS: Description of sLH2 concept, modelling approach and results of numerical simulations. *International Journal of Hydrogen Energy*. 93. 285–296. 2024
16. Sivaraman, S., Makarov, D., and Molkov, V. Flash boiling and pressure recovery phenomenon during venting from liquid ammonia tank ullage. *Process Safety and Environmental Protection*. 182. 880–893. 2024
17. Molkov, V., Sivaraman, S., Cirrone, D., Truchot, B., and Makarov, D. Modelling and numerical simulations of heat and mass transfer in multiphase flow during the release of liquid ammonia from a storage tank through the piping system to the open atmosphere. *International Journal of Heat and Mass Transfer*. 246. 2025
18. Kharangate, C.R. and Mudawar, I. Review of computational studies on boiling and condensation. *International Journal of Heat and Mass Transfer*. 108. 1164–1196. 2017
19. Li, J., Liang, G., Zhu, P., and Wang, X. Numerical investigation of the operating process of the liquid hydrogen tank under gaseous hydrogen pressurization. *Aerospace Science and Technology*. 93. 105327. 2019
20. Ma, Y., Li, Y., Zhu, K., Wang, Y., Wang, L., and Tan, H. Investigation on no-vent filling process of liquid hydrogen tank under microgravity condition. *International Journal of Hydrogen Energy*. 42, no. 12. 8264–8277. 2017
21. Kim, Y., Choi, J., Kim, S., and Zhang, Y. Effects of mass transfer time relaxation parameters on condensation in a thermosyphon. *Journal of Mechanical Science and Technology*. 29, no. 12. 5497–5505. 2015
22. Hou, C., Yu, Y., Liu, X., Ding, J., and Cui, Z. Effects of longitudinal excitation on liquid hydrogen sloshing in spacecraft storage tanks under microgravity conditions. *International Journal of Hydrogen Energy*. 51. 765–780. 2024

23. Shu, Z.Y., Lei, G., Liang, W.Q., Wang, T.X., and Qian, H. Investigation of Hydrogen Dispersion Characteristics with Liquid Helium Spills. *Journal of Physics: Conference Series*. 2208, no. 1. 012020. 2022
24. NIST. Isobaric Properties for Helium. *https://webbook.nist.gov/cgi/fluid.cgi?P=0.101325&TLow=4.15&THigh=300&TInc=1&Digits=5&ID=C7440597&Action=Load&Type=IsoBar&TUnit=K&PUnit=MPa&DUnit=kg%2Fm3&HUnit=kJ%2Fmol&WUnit=m%2Fs&VisUnit=Pa*s&STUnit=dyn%2Fcm&RefState=DEF*